Two-loop photon self-energy in pseudoquantum electrodynamics in the presence of a conducting surface

Danilo C. Pedrelli,[*] Danilo T. Alves,[†] and Van Sérgio Alves[‡]
Faculdade de Física, Universidade Federal do Pará, 66075-110 Belém, Brazil

(Received 4 October 2020; accepted 6 December 2020; published 30 December 2020)

In the present paper, we investigate the influence of a grounded perfectly conducting surface on the photon self-energy of a $2+1$D system of massless Dirac fermions, whose electron interaction is described by pseudoquantum electrodynamics. We calculate the temporal component of the polarization tensor up to 2-loop perturbation order in the presence of the conducting surface and, applying the Kubo formula, we obtain the longitudinal and optical conductivities of such system. When the distance between the system and the plate tends to infinity, we recover the correspondent results found in the literature. Since pseudoquantum electrodynamics proved to give a good description of the transport properties of graphene, our results can be useful as an alternative way to control the longitudinal and optical conductivities of this material.

DOI: 10.1103/PhysRevD.102.125032

I. INTRODUCTION

Recently, quantum field theories in $2+1$D have been extensively studied. This interest is due, in part, to their potential applications in the physics of condensed matter, such as, for instance, the quantum Hall effect [1] and the theory of superconductivity with a high critical temperature value [2–4]. The discovery of graphene has provided a fascinating possibility to relate relativistic quantum field theories to a condensed matter system [5]. In this material, the valence electrons are originated in $sp2$ orbitals (σ-type bonds) and p_z orbitals (π-type bonds). However, since the electrons of p_z orbitals are weakly bound to the atoms, they are effectively the most important electrons for the optical and electrical transport properties of graphene [5]. Besides that, the electronic dispersion of graphene exhibits a particle-hole symmetry and, for low energies, a linear dependence on the momentum $\mathbf{k}$ is observed, $E_{\pm}(\mathbf{k}) \approx \pm v_F|\mathbf{k}|$ [6], where v_F is the bare Fermi velocity. These characteristics allow us to relate the p_z electrons in graphene to free Dirac massless particles in $2+1$D (hereafter we refer to the $2+1$D system of massless Dirac fermions as $2+1$D system). The fact that electrons in graphene are relativistic opened the possibility of predicting, in this material, typical phenomena of particle physics. In this sense, some phenomena, such as Klein's paradox [7–10], and *Zitterbewegung* [11,12], are examples known to occur in graphene. In addition, graphene also exhibits an unconventional transport phenomenon, characterized by the existence of the anomalous quantum Hall effect [13] and minimal dc conductivity, whose value in the approximation of noninteracting electrons is given by $(\pi/2)e^2/h$ [14]. Since the relevance of electronic interactions in graphene was confirmed by the experimental observation of the renormalization of the Fermi velocity [15], as predicted in Ref. [16] with a theory that considered such interactions, there has been a great effort in trying to obtain models that describe some physical properties of these materials.

The electronic interaction between p_z electrons in graphene is described by the minimal coupling between the electronic current and the gauge field. However, this is not easily incorporated into the model, because the electrons in graphene are constrained to move in a $2+1$D plane, whereas the photon lives in $3+1$D. The usual quantum electrodynamics in $2+1$D is not a good candidate to describe such a system, because for this theory both electrons and photons are confined to the plane. Furthermore, this theory produces an interaction between electrons proportional to $\ln r$ [17] (nonphysical), instead of the Coulomb potential $1/r$. An appropriate gauge theory that has the characteristic of mixing dimensions is pseudoquantum electrodynamics (PQED) [18], also known as reduced quantum electrodynamics [19], which is the projection of QED4 on the plane and leads to a nonlocal gauge field. This approach provides the correct propagator of the gauge field and properly accounts for several features, such as scale invariance [20]. In particular, it has been shown that these models respect causality [21] and unitarity [22]. Indeed, the gauge field propagator in PQED has support in the

[*]danilo.pedrelli@icen.ufpa.br
[†]danilo@ufpa.br
[‡]vansergi@ufpa.br

light-cone surface and therefore the theory obeys the Huygens principle, as in the case of QED4, and in contrast to QED3 [23]. Furthermore, PQED yields the Coulomb potential in the static limit, which is a desirable feature for applications in the physics of two-dimensional materials [24].

When the dimensional reduction from the QED4 to PQED takes into account the effects of boundary conditions imposed to the electromagnetic field in $3+1$D, the influence of such external conditions is carried into PQED, producing the so-called cavity PQED [25,26]. In this context, Silva *et al.* [25], showed that the renormalization of the Fermi velocity is inhibited by the presence of a grounded perfectly conducting surface. Such effect, caused by a modification in the photon propagator by the conducting surface, should also have an influence on the polarization tensor, which, using the Kubo formula, determines the longitudinal conductivity, and, in the low momentum limit, results in the optical conductivity of the system [27].

In the present paper, we investigate how the conducting plate and its distance to the $2+1$D system affect the photon self-energy, which, as mentioned, results in a modification of the conductivity. More specifically, we compute the 2-loop contributions to the 00-component of the polarization tensor for the $2+1$D system in the presence of a grounded perfectly conducting plate. From this result, the longitudinal and optical conductivities are obtained, according to the Kubo formula.

The paper is organized as follows. In Sec. II, we present the model and the Feynman rules. In Sec. III, we review the influence of a conducting surface on the renormalized Fermi velocity in the static regime, obtained in Ref. [25]. In Sec. IV, we calculate the polarization tensor at 2-loop perturbation order in the presence of the conducting surface. In Sec. V, we merge all results and get the longitudinal conductivity. Also, the optical limit of the conductivity is investigated. In Sec. VI, we analyze our results and make final comments.

II. THE MODEL AND FEYNMAN RULES

PQED, which was first proposed by Marino [18], describes the electromagnetic interaction between electrons moving on a plane in a $2+1$D spacetime. In PQED, although electrons are confined to a plane, they interact, effectively, as particles in $3+1$D. Formally, this system can be achieved by changing the usual Maxwell term $F_{\mu\nu}^2$ by $F_{\mu\nu}^2/\sqrt{-\Box}$, where $\Box$ is the d'Alembertian operator. Besides that, since the nonlocal gauge field also produces the full electromagnetic interaction, independently of whether the matter is relativistic or not, we can easily include the Lorentz symmetry breaking term in the matter field. Considering this, we start with anisotropic PQED, given by the effective Lagrangian ($\hbar = c = 1$)

$$\mathcal{L}_{\mathrm{PQED}} = \frac{F_{\mu\nu}F^{\mu\nu}}{2(-\Box)^{1/2}} + \bar{\psi}_a(i\gamma^0\partial_0 + iv_F\gamma\cdot\nabla)\psi_a + j^\mu A_\mu - \frac{\xi}{2}A_\mu\frac{\partial^\mu\partial^\nu}{(-\Box)^{1/2}}A_\nu, \tag{1}$$

where $F_{\mu\nu}$ is the usual electromagnetic tensor, v_F is the bare Fermi velocity of the electrons in the $2+1$D system, $\psi_a^\dagger = (\psi_{A\uparrow}^*\psi_{A\downarrow}^*\psi_{B\uparrow}^*\psi_{B\downarrow}^*)_a$ is the four-component Dirac spinor representation of the electrons The flavor index a represents a sum over valleys $\mathcal{K}$ and $\mathcal{K}'$, A and B denote the sublattices in graphene, whereas $\uparrow$ and $\downarrow$ are the different spin orientations [23,25,26,28]. $\gamma^\mu = (\gamma^0, v_F\gamma)$ are rank-4 Dirac matrices, j^μ is the matter current in $2+1$D, and the last term is the gauge fixing. PQED has been successfully used in the description of several properties $2+1$D systems [24–26,28–37].

Considering Eq. (1), the photon propagator is given by [29]

$$\Delta_{\mu\nu}^{(0)}(k) = \frac{2\pi}{\kappa\sqrt{k^2}}\left[\delta_{\mu\nu} - \left(1-\frac{1}{\xi}\right)\frac{k_\mu k_\nu}{k^2}\right], \tag{2}$$

where κ is the dielectric constant of the environment in cgs units, and we defined the quadrimomentum $k = (k_0, \mathbf{k})$, with $\not{k} = \gamma^0 k_0 + v_F\gamma\cdot\mathbf{k}$ and $k^2 = k_0^2 + v_F^2|\mathbf{k}|^2$. Also, since we are working in the Euclidean space representation, the γ matrices satisfy $\{\gamma^\mu, \gamma^\nu\} = 2\delta^{\mu\nu}\mathbf{I}$, where $\mu, \nu = 0, 1, 2$ and $\mathbf{I} = \mathrm{diag}(1,1,1)$ [38].

Assuming the Feynman gauge ($\xi = 1$) and the static regime ($k_0 = 0$), we get

$$\Delta_{\mu\nu}^{(0)}(|\mathbf{k}|) = \frac{2\pi}{\kappa|\mathbf{k}|}\delta_{0\mu}\delta_{0\nu}, \tag{3}$$

which, by a Fourier transform [17], leads to the Coulombian potential for static charges,

$$V(|\mathbf{r}|) = \frac{e}{\kappa|\mathbf{r}|}, \tag{4}$$

where e is the bare coupling constant and $|\mathbf{r}|$ is the distance between an electron and a point where the potential is calculated. The bare fermion propagator is defined as

$$S_F^{(0)}(k) = \frac{\gamma^0 k_0 + v_F\gamma\cdot\mathbf{k}}{k_0^2 + v_F^2|\mathbf{k}|^2}. \tag{5}$$

From (3), the electron self-energy becomes [39]

$$\Sigma(\mathbf{q}) = -\frac{e^2}{4\kappa}\mathbf{q}\cdot\gamma\ln\left(\frac{\Lambda}{|\mathbf{q}|}\right), \tag{6}$$

where Λ is the ultraviolet momentum cutoff. Note that, since we considered the static approximation, there is no wave function renormalization at the 1-loop order [39].

From Eq. (6), one obtains the renormalized Fermi velocity [39]

$$v_{\mathbf{q}}^{*} = v_F\left[1+\frac{\alpha}{4}\ln\left(\frac{\Lambda}{|\mathbf{q}|}\right)\right], \tag{7}$$

where $\alpha = e^2/(\kappa v_F)$ is the fine structure constant of the $2+1$D system. Consequently, the renormalized α will be [38]

$$\alpha_{\mathbf{q}}^{*} = \frac{\alpha}{1+\frac{\alpha}{4}\ln(\Lambda/|\mathbf{q}|)}. \tag{8}$$

III. THE EFFECT OF THE CONDUCTING SURFACE IN THE STATIC REGIME

Among the various ways to influence the transport properties of graphene (see [5,40]), it has been shown by Silva *et al.* [25,26] that a grounded perfectly conducting surface can inhibit the renormalization of the Fermi velocity in a neutral graphene sheet placed in vacuum (see Fig. 1, $\kappa = 1$ for vacuum). In this context, we can also highlight the work of Raoux *et al.* [41], who obtained, for doped graphene, the inhibition of the renormalized Fermi velocity in the same configuration.

Considering Fig. 2, an electron (charge e) in the $2+1$D system (located at the point P), in the presence of a parallel grounded perfectly conducting plate at a distance ρ_0, interacts not only with another electron in the same sheet (at point A), but also with a certain amount of positive charge on the surface of the conducting plate induced by the other electron (at point A'). Using the image method, this amount of positive charge is effectively given by an image charge $e' = -e$. Taking this into account, the resultant static potential will be given by [25,26]

$$V(\rho_0, |\mathbf{r}|) = \frac{e}{\kappa}\left[\frac{1}{|\mathbf{r}|} - \frac{1}{\sqrt{|\mathbf{r}|^2+(2\rho_0)^2}}\right]. \tag{9}$$

Taking a Fourier transform over Eq. (9), the photon propagator becomes [25,26]

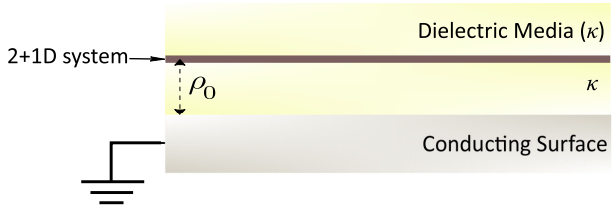

FIG. 1. A $2+1$D system of massless Dirac fermions at a distance ρ_0 from a grounded perfectly conducting surface. The dielectric media above and below the $2+1$D system have the same dielectric constant κ.

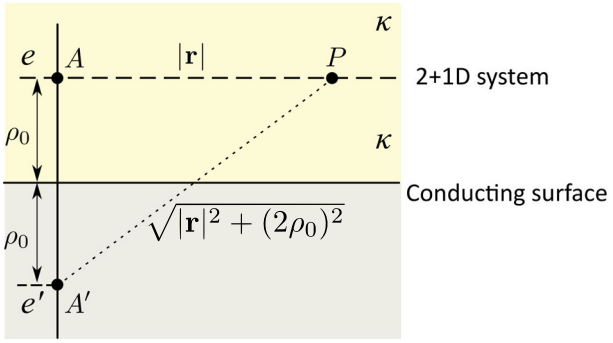

FIG. 2. Illustration of the $2+1$D system, represented by the dashed line, located at a distance ρ_0 from the conducting surface (represented by the solid horizontal line). An electron e in the $2+1$D system, located at the point A, has its image $e' = -e$ at the point A'. P is the point in the $2+1$D system where the potential is computed.

$$\Delta_{00}^{(0)}(\rho_0, |\mathbf{k}|) = \frac{2\pi}{\kappa|\mathbf{k}|}(1-e^{-2\rho_0|\mathbf{k}|}). \tag{10}$$

Considering Eq. (10), the electron self-energy correction is [25]

$$\Sigma(\rho_0, \mathbf{q}) = -\frac{e^2}{4\kappa}\mathbf{q}\cdot\gamma\left[\ln\left(\frac{\Lambda}{|\mathbf{q}|}\right) - F(\rho_0|\mathbf{q}|, \Lambda)\right], \tag{11}$$

where

$$F(\rho_0|\mathbf{q}|, \Lambda) = \frac{1}{2\pi}\int_0^{2\pi} d\zeta \int_0^{\xi_\Lambda} d\xi (1+\cosh\xi\cos\zeta) \times \exp[-\rho_0|\mathbf{q}|(\cosh\xi - \cos\zeta)], \tag{12}$$

and

$$\xi_\Lambda = \cosh^{-1}\left(\frac{2\Lambda}{|\mathbf{q}|} + \cos\zeta\right). \tag{13}$$

Hence, the renormalized Fermi velocity will be written as [25]

$$v_{\rho_0,\mathbf{q}}^{*} = v_F\left\{1+\frac{\alpha}{4}\left[\ln\left(\frac{\Lambda}{|\mathbf{q}|}\right) - F(\rho_0|\mathbf{q}|, \Lambda)\right]\right\}. \tag{14}$$

Next, we compute the influence of the conducting surface on the polarization tensor.

IV. POLARIZATION TENSOR

The component Π^{00}, renamed as Π, can be expanded perturbatively as

$$\Pi(\omega, \mathbf{q}) \approx \Pi_1(\omega, \mathbf{q}) + 2\Pi_{2a}(\omega, \mathbf{q}) + \Pi_{2b}(\omega, \mathbf{q}), \tag{15}$$

where Π_1 is the contribution coming from the 1-loop Feynman diagram [see Fig. 3(a)], whereas Π_{2a} [Fig. 3(b)] and Π_{2b} [Fig. 3(b)] are contributions from the 2-loop diagrams. Due to its symmetry, the correction Π_{2a} must be multiplied by the factor 2.

From Fig. 3(a), one can see that there are no photon lines in the Π_1 diagram, therefore, the result is the same for QED in 2 + 1D, given by [38,42,43]

$$\Pi_1(\omega,\mathbf{q}) = -\frac{Ne^2|\mathbf{q}|}{8v_F}\frac{1}{\sqrt{1-y_q^2}}, \tag{16}$$

where $N = 2$ corresponds to the $\mathcal{K}$ and $\mathcal{K}'$ valleys, and we defined $iq_0 = \omega + i\epsilon$, $\epsilon \to 0^+$, with $y_q = (\omega + i\epsilon)/v_F|\mathbf{q}|$ (remember that $q = (q_0, \mathbf{q})$ represents the quadrimomentum).

The diagrams in Figs. 3(b) and 3(c) show that these contributions to Π depend on the photon propagator and, therefore, are directly affected by the presence of the conducting plate [to emphasize this influence, hereafter, we write $\Pi_{2a}(\rho_0,\omega,\mathbf{q})$ and $\Pi_{2b}(\rho_0,\omega,\mathbf{q})$].

A. Calculation of Π_{2a}

The diagram presented in Fig. 3(b) leads to the following definition:

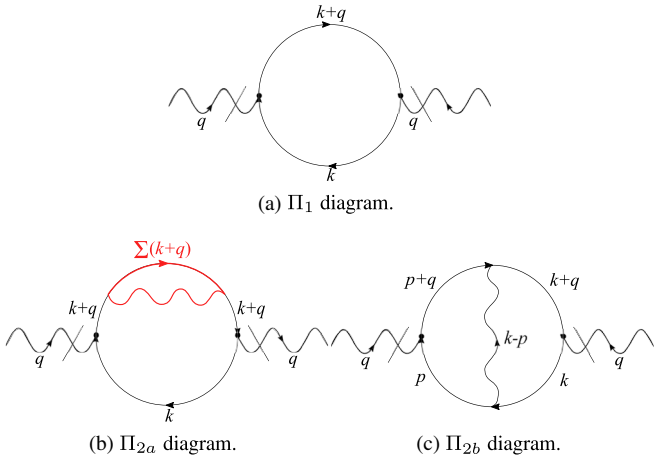

FIG. 3. Feynman diagrams representing the first terms of the perturbative expansion of Π, according to Eq. (15). The red part of the diagram in (b) is to highlight the contribution of the electron self-energy diagram.

$$\Pi_{2a}(\rho_0,\omega,\mathbf{q}) = -N\int\frac{d^3k}{(2\pi)^3}\mathrm{Tr}[e\gamma^0 S_F^{(0)}(k)e\gamma^0 S_F^{(0)}(k+q) \times \Sigma(\rho_0,\mathbf{k}+\mathbf{q})S_F^{(0)}(k+q)], \tag{17}$$

which, from Eqs. (5), (10) and (11), gives

$$\Pi_{2a}(\rho_0,\omega,\mathbf{q}) = Ne^2\int\frac{d^3k}{(2\pi)^3}\mathrm{Tr}\left\{\gamma^0\frac{\not{k}}{k^2}\gamma^0\frac{(\not{k}+\not{q})}{(k+q)^2}\frac{e^2}{4\kappa}(\mathbf{k}+\mathbf{q})\cdot\gamma\left[\ln\left(\frac{\Lambda}{|\mathbf{k}+\mathbf{q}|}\right) - F(\rho_0|\mathbf{k}+\mathbf{q}|,\Lambda)\right]\frac{(\not{k}+\not{q})}{(k+q)^2}\right\}. \tag{18}$$

Following the same approach of Ref. [38], one can find that

$$\Pi_{2a}(\rho_0,\omega,\mathbf{q}) = -\frac{Ne^4}{2\kappa}\int\frac{d^2k}{(2\pi)^2}\frac{\mathbf{k}\cdot(\mathbf{k}+\mathbf{q}) - |\mathbf{k}||\mathbf{k}+\mathbf{q}|}{|\mathbf{k}|}\frac{[v_F^2(|\mathbf{k}|+|\mathbf{k}+\mathbf{q}|)^2 - q_0^2]}{[v_F^2(|\mathbf{k}|+|\mathbf{k}+\mathbf{q}|)^2 + q_0^2]^2}\left[\ln\left(\frac{\Lambda}{|\mathbf{k}+\mathbf{q}|}\right) - F(\rho_0|\mathbf{k}+\mathbf{q}|,\Lambda)\right]. \tag{19}$$

By making $\mathbf{k} \to -\mathbf{k} - \mathbf{q}$, choosing a coordinate system such that $\mathbf{q} = (|\mathbf{q}|, 0)$, and performing a transformation to elliptic coordinates [38,44],

$$k_x = \frac{|\mathbf{q}|}{2}(\cosh\mu\cos\nu - 1), \qquad k_y = \frac{|\mathbf{q}|}{2}\sinh\mu\sin\nu, \qquad d^2k = \frac{|\mathbf{q}|^2}{4}(\cosh^2\mu - \cos^2\nu)d\mu d\nu, \tag{20}$$

we are able to obtain

$$\Pi_{2a}(\rho_0,\omega,\mathbf{q}) = \frac{Ne^4|\mathbf{q}|}{32\pi^2\kappa v_F^2}\int_0^{2\pi}d\nu\int_0^{\infty}d\mu\frac{\sin^2\nu(\cosh\mu-\cos\nu)(\cosh^2\mu+y_q^2)}{(\cosh^2\mu-y_q^2)^2}\left[\ln\left(\frac{2\Lambda}{|\mathbf{q}|(\cosh\mu-\cos\nu)}\right) - F\left(\frac{\rho_0|\mathbf{q}|}{2}(\cosh\mu-\cos\nu),\Lambda\right)\right]. \tag{21}$$

The above equation can be rewritten as

$$\Pi_{2a}(\rho_0,\omega,\mathbf{q})=\frac{e^2\alpha|\mathbf{q}|}{16\pi v_F}\left[\frac{\pi}{2}\frac{1}{(1-y_q^2)^{3/2}}\ln(\Lambda/|\mathbf{q}|)+I_{a'}(y_q)-I_{a''}(\rho_0|\mathbf{q}|,y_q,\Lambda)\right], \tag{22}$$

where the function $I_{a'}(y_q)$ was obtained in Ref. [44]:

$$I_{a'}(y_q)=\frac{1}{3}\frac{1+2y_q^2}{1-y_q^2}-\frac{y_q}{6}\frac{5-2y_q^2}{1-y_q^2}\ln\left(\frac{1-y_q}{1+y_q}\right)-\frac{\pi}{12}\frac{3-12\ln 2+6y_q^2-4y_q^4}{(1-y_q^2)^{3/2}}-\frac{i}{(1-y_q^2)^{3/2}}$$
$$\times\left[\frac{\pi^2}{4}-\mathrm{Li}_2\left(y_q+i\sqrt{1-y_q^2}\right)+\mathrm{Li}_2\left(-y_q-i\sqrt{1-y_q^2}\right)+\frac{i\pi}{2}\ln\left(y_q+i\sqrt{1-y_q^2}\right)\right], \tag{23}$$

where $\mathrm{Li}_2(z)=\sum_{k=1}^{\infty}z^k/k^2$ is the dilogarithmic function, whereas $I_{a''}(\rho_0|\mathbf{q}|,y_q,\Lambda)$ is the following integral, which will be solved numerically:

$$I_{a''}(\rho_0|\mathbf{q}|,y_q,\Lambda)=\int_0^{2\pi}d\nu\int_0^{\infty}d\mu\frac{\sin^2\nu(\cosh\mu-\cos\nu)(\cosh^2\mu+y_q^2)}{\pi(\cosh^2\mu-y_q^2)^2}F\left(\frac{\rho_0|\mathbf{q}|}{2}(\cosh\mu-\cos\nu),\Lambda\right). \tag{24}$$

Defining $x_q=\mathrm{Re}y_q=\omega/(v_F|\mathbf{q}|)$, we see that, for $x_q>1$, there is a pole on the contour. In such situation, we can determine the real and imaginary parts of $I_{a''}(\rho_0|\mathbf{q}|,y_q,\Lambda)$ using a generalization of the Sokhotski-Plemelj identity for integrals with higher order poles [45], as presented in Appendix A 1:

$$\mathrm{Re}I_{a''}(\rho_0|\mathbf{q}|,x_q,\Lambda)=\lim_{\epsilon\to0^+}\int_0^{2\pi}d\nu\left[\int_1^{x_q-\epsilon}\frac{H(w,x_q,\nu)}{(w-x_q)^2}dw+\int_{x_q+\epsilon}^{\infty}\frac{H(w,x_q,\nu)}{(w-x_q)^2}dw-\frac{2H(x_q,x_q,\nu)}{\epsilon}\right], \tag{25}$$

$$\mathrm{Im}I_{a''}(\rho_0|\mathbf{q}|,x_q,\Lambda)=\int_0^{2\pi}d\nu\left.\frac{dH(w,x_q,\nu)}{dw}\right|_{w=x_q}, \tag{26}$$

where $w=\cosh\mu$ and

$$H(w,x_q,\nu)=\frac{1}{\pi}\frac{\sin^2\nu(w-\cos\nu)(w^2+x_q^2)}{(w+x_q)^2\sqrt{w^2-1}}F\left(\frac{\rho_0|\mathbf{q}|}{2}(w-\cos\nu),\Lambda\right). \tag{27}$$

B. Calculation of Π_{2b}

The diagram in Fig. 3(c) leads to the following polarization correction:

$$\Pi_{2b}(\rho_0,\omega,\mathbf{q})=-Ne^4\iint\frac{d^3k}{(2\pi)^3}\frac{d^3p}{(2\pi)^3}\Delta_{00}^{(0)}(\rho_0,|\mathbf{k}-\mathbf{p}|)\mathrm{Tr}[\gamma^0S_F^{(0)}(p+q)\gamma^0S_F^{(0)}(k+q)\gamma^0S_F^{(0)}(k)\gamma^0S_F^{(0)}(p)], \tag{28}$$

which, according to Eqs. (10) and (5), gives

$$\Pi_{2b}(\rho_0,\omega,\mathbf{q})=-\frac{2\pi e^4N}{\kappa}\iint\frac{d^3k}{(2\pi)^3}\frac{d^3p}{(2\pi)^3}\frac{1-e^{-2\rho_0|\mathbf{k}-\mathbf{p}|}}{|\mathbf{k}-\mathbf{p}|}\mathrm{Tr}\left[\gamma^0\frac{(\not{p}+\not{q})}{(p+q)^2}\gamma^0\frac{(\not{k}+\not{q})}{(k+q)^2}\gamma^0\frac{\not{k}}{k^2}\gamma^0\frac{\not{p}}{p^2}\right]. \tag{29}$$

Considering Ref. [38], we find

$$\Pi_{2b}(\rho_0,\omega,\mathbf{q})=-\frac{2\pi Ne^4}{\kappa}\iint\frac{d^2k}{(2\pi)^2}\frac{d^2p}{(2\pi)^2}\frac{1-e^{-2\rho_0|\mathbf{k}-\mathbf{p}|}}{|\mathbf{k}-\mathbf{p}|[v_F^2(|\mathbf{k}|+|\mathbf{k}+\mathbf{q}|)^2+q_0^2][v_F^2(|\mathbf{p}|+|\mathbf{p}+\mathbf{q}|)^2+q_0^2]}$$
$$\times\left\{-q_0^2\left(\frac{\mathbf{k}\cdot\mathbf{p}}{|\mathbf{k}||\mathbf{p}|}-\frac{\mathbf{p}\cdot(\mathbf{k}+\mathbf{q})}{|\mathbf{p}||\mathbf{k}+\mathbf{q}|}-\frac{\mathbf{k}\cdot(\mathbf{p}+\mathbf{q})}{|\mathbf{k}||\mathbf{p}+\mathbf{q}|}+\frac{(\mathbf{k}+\mathbf{q})\cdot(\mathbf{p}+\mathbf{q})}{|\mathbf{k}+\mathbf{q}||\mathbf{p}+\mathbf{q}|}\right)\right.$$
$$+\frac{v_F^2(|\mathbf{k}|+|\mathbf{k}+\mathbf{q}|)(|\mathbf{p}|+|\mathbf{p}+\mathbf{q}|)}{|\mathbf{k}||\mathbf{p}||\mathbf{k}+\mathbf{q}||\mathbf{p}+\mathbf{q}|}[\mathbf{k}\cdot\mathbf{p}|\mathbf{q}|^2-(\mathbf{k}\cdot\mathbf{q})(\mathbf{p}\cdot\mathbf{q})$$
$$\left.+(|\mathbf{k}|^2+\mathbf{k}\cdot\mathbf{q}-|\mathbf{k}||\mathbf{k}+\mathbf{q}|)(|\mathbf{p}|^2+\mathbf{p}\cdot\mathbf{q}-|\mathbf{p}||\mathbf{p}+\mathbf{q}|)]\right\}. \tag{30}$$

By making a transformation to elliptic coordinates over momenta $\mathbf{k}$ and $\mathbf{p}$, in the same way of Eq. (20), we get

$$\Pi_{2b}(\rho_0,\omega,\mathbf{q}) = -\frac{Ne^2|\mathbf{q}|\alpha}{16\pi^3 v_F}\int \frac{d\mu d\mu' d\nu d\nu' \cosh\mu\cosh\mu'\sin\nu\sin\nu'}{\sqrt{[\cosh(\mu+\mu')-\cos(\nu+\nu')][\cosh(\mu-\mu')-\cos(\nu-\nu')]}} \times \frac{[\sin\nu\sin\nu' + \sinh\mu\sinh\mu' + y_q^2(\sin\nu\sin\nu' + \tanh\mu\tanh\mu'\cos\nu\cos\nu')]}{(\cosh^2\mu - y_q^2)(\cosh^2\mu' - y_q^2)} \times \left[1 - \exp\left(-\rho_0|\mathbf{q}|\sqrt{[\cosh(\mu+\mu')-\cos(\nu+\nu')][\cosh(\mu-\mu')-\cos(\nu-\nu')]}\right)\right]. \tag{31}$$

After that, making $\eta = \nu + \nu'$, $\tau = \nu - \nu'$, $a = \mu + \mu'$ and $b = \mu - \mu'$, we find:

$$\Pi_{2b}(\rho_0,\omega,\mathbf{q}) = \frac{|\mathbf{q}|e^2\alpha}{v_F} p_{2b}(\rho_0|\mathbf{q}|, y_q), \tag{32}$$

where

$$p_{2b}(\rho_0|\mathbf{q}|, y_q) = -\frac{1}{16\pi^3}\int_0^\infty db\int_b^\infty da \frac{1}{[1-2y_q^2+\cosh(a+b)][1-2y_q^2+\cosh(a-b)]} \times [(\cosh^2 a - \cosh^2 b)(1+y_q^2)M_1(a,b,\rho_0|\mathbf{q}|) + (\cosh a + \cosh b)M_2(a,b,\rho_0|\mathbf{q}|) + y_q^2(\cosh a - \cosh b)M_3(a,b,\rho_0|\mathbf{q}|)], \tag{33}$$

and

$$M_i(a,b,\rho_0|\mathbf{q}|) = \int_0^{2\pi} d\eta \int_0^{2\pi} d\tau h_i(1 - h_{\rho_0|\mathbf{q}|}), \quad \text{for } i = 1,2,3, \tag{34}$$

with

$$h_1 = \frac{\cos\tau - \cos\eta}{\sqrt{[\cosh a - \cos\eta][\cosh b - \cos\tau]}}, \qquad h_2 = \frac{(\cos\tau - \cos\eta)^2}{\sqrt{[\cosh a - \cos\eta][\cosh b - \cos\tau]}}, \tag{35}$$

$$h_3 = \frac{\cos^2\tau - \cos^2\eta}{\sqrt{[\cosh a - \cos\eta][\cosh b - \cos\tau]}}, \qquad h_{\rho_0|\mathbf{q}|} = \exp\left(-\rho_0|\mathbf{q}|\sqrt{[\cosh a - \cos\eta][\cosh b - \cos\tau]}\right). \tag{36}$$

The integral in Eq. (33) has a pole at $x_q > 1$. Therefore, within this region, we split the integral into real and imaginary parts with the application of the Sokhotski-Plemelj identity (as shown in Appendix A 2), resulting in

$$\mathrm{Re}[p_{2b}(\rho_0|\mathbf{q}|, x_q)] = -\frac{1}{16\pi^3}\lim_{\epsilon\to 0^+}\int_0^\infty db\left[\int_b^{\lambda(x_q)-b-\epsilon} da \frac{U(a,b,\rho_0|\mathbf{q}|,\lambda(x_q))}{g_+(a,b,\lambda(x_q))g_-(a,b,\lambda(x_q))} + \int_{\lambda(x_q)-b+\epsilon}^{\lambda(x_q)+b-\epsilon} da \frac{U(a,b,\rho_0|\mathbf{q}|,\lambda(x_q))}{g_+(a,b,\lambda(x_q))g_-(a,b,\lambda(x_q))} + \int_{\lambda(x_q)+b+\epsilon}^{\infty} da \frac{U(a,b,\rho_0|\mathbf{q}|,\lambda(x_q))}{g_+(a,b,\lambda(x_q))g_-(a,b,\lambda(x_q))}\right], \tag{37}$$

$$\mathrm{Im}[p_{2b}(\rho_0|\mathbf{q}|, x_q)] = -\frac{1}{32\pi^2\sinh(\lambda(x_q))}\left\{\int_0^{\lambda(x_q)/2}\frac{db}{\sinh b}\left[\frac{U(\lambda(x_q)+b,b,\rho_0|\mathbf{q}|,\lambda(x_q))}{\sinh(b+\lambda(x_q))} - \frac{U(\lambda(x_q)-b,b,\rho_0|\mathbf{q}|,\lambda(x_q))}{\sinh(\lambda(x_q)-b)}\right] + \int_{\lambda(x_q)/2}^\infty \frac{db}{\sinh b}\frac{U(\lambda(x_q)+b,b,\rho_0|\mathbf{q}|,\lambda(x_q))}{\sinh(b+\lambda(x_q))}\right\}, \tag{38}$$

where we have defined $x_q = \cosh(\lambda/2)$ as in Ref. [44], and

$$U(a,b,\rho_0|\mathbf{q}|,\lambda) = (\cosh^2 a - \cosh^2 b)M_1(a,b,\rho_0|\mathbf{q}|) + \left(\frac{\cosh\lambda + 3}{2}\right)(\cosh a + \cosh b)M_2(a,b,\rho_0|\mathbf{q}|) + \frac{\cosh\lambda + 1}{2}(\cosh a - \cosh b)M_3(a,b,\rho_0|\mathbf{q}|), \tag{39}$$

with

$$g_+(a,b,\lambda) = \cosh(a+b) - \cosh\lambda, \tag{40}$$

and

$$g_-(a,b,\lambda) = \cosh(a-b) - \cosh\lambda. \tag{41}$$

C. Renormalization

Until here, we have written the polarization tensor in terms of the bare parameters α and v_F. However, in order to have results written in terms of observable quantities, we must rewrite the polarization tensor in terms of renormalized parameters, as stated in Refs. [38,44]. The method to do this transformation, as described in Refs. [38,44,46], is to perform the summation $\Pi_1 + 2\Pi_{2a}$ and absorb the logarithmic divergence into the renormalized Fermi velocity. Following this method, and considering the conducting surface, the combination of Eqs. (16) and (22) leads to

$$\Pi_1(\omega,\mathbf{q}) + 2\Pi_{2a}(\rho_0,\omega,\mathbf{q}) = -\frac{Ne^2|\mathbf{q}|}{8v_F}\left\{\frac{1}{\sqrt{1-y_q^2}} - \frac{\alpha}{4}\frac{1}{(1-y_q^2)^{3/2}}[\ln(\Lambda/|\mathbf{q}|) - F(\rho_0|\mathbf{q}|,\Lambda)] - \frac{\alpha}{4}\frac{F(\rho_0|\mathbf{q}|,\Lambda)}{(1-y_q^2)^{3/2}} - \frac{\alpha}{2\pi}[I_{a'}(y_q) - I_{a''}(\rho_0|\mathbf{q}|,y_q,\Lambda)]\right\}, \tag{42}$$

where, for convenience, we added and subtracted $Ne^2|\mathbf{q}|\alpha F(\rho_0|\mathbf{q}|,\Lambda)/[32v_F(1-y_q^2)^{3/2}]$ to the right-hand side.

Now, considering the renormalized Fermi velocity in Eq. (14) and the renormalized fine structure constant of the $2+1$D system in the presence of a conducting plate,

$$\alpha^*_{\rho_0,\mathbf{q}} = \frac{e^2}{\kappa v^*_{\rho_0,\mathbf{q}}} = \frac{\alpha}{1+\frac{\alpha}{4}[\ln(\Lambda/|\mathbf{q}|) - F(\rho_0|\mathbf{q}|,\Lambda)]}, \tag{43}$$

we write α in terms of $\alpha^*_{\rho_0,\mathbf{q}}$,

$$\alpha = \alpha^*_{\rho_0,\mathbf{q}}\left\{1 + \frac{\alpha^*_{\rho_0,\mathbf{q}}}{4}[\ln(\Lambda/\mathbf{q}) - F(\rho_0|\mathbf{q}|,\Lambda)]\right\} + \mathcal{O}(\alpha^{*3}_{\rho_0,\mathbf{q}}). \tag{44}$$

Then, replacing the above equation into Eq. (42) and performing a series expansion until $\mathcal{O}(\alpha^*_{\rho_0,\mathbf{q}})$, one can show that the combination of terms leads to the absorption of the logarithmic divergence into the renormalized Fermi velocity and Eq. (42) becomes

$$\Pi_1(\omega,\mathbf{q}) + 2\Pi_{2a}(\rho_0,\omega,\mathbf{q}) \approx -\frac{e^2|\mathbf{q}|}{4v^*_{\rho_0,\mathbf{q}}\sqrt{1-y^{*2}_{\rho_0,q}}} + \frac{e^2|\mathbf{q}|\alpha^*_{\rho_0,\mathbf{q}}}{v^*_{\rho_0,\mathbf{q}}}p_{2a}(\rho_0|\mathbf{q}|,y^*_{\rho_0,q}), \tag{45}$$

where

$$p_{2a}(\rho_0|\mathbf{q}|,y^*_{\rho_0,q}) = \frac{1}{8\pi}\left[\frac{\pi}{2}\frac{F(\rho_0|\mathbf{q}|,\Lambda)}{(1-y^{*2}_{\rho_0,q})^{3/2}} + I_{a'}(y^*_{\rho_0,q}) - I_{a''}(\rho_0|\mathbf{q}|,y^*_{\rho_0,q})\right], \tag{46}$$

$$y^*_{\rho_0,q} = x^*_{\rho_0,q} + i\epsilon, \quad \text{and} \quad x^*_{\rho_0,q} = \frac{\omega}{v^*_{\rho_0,\mathbf{q}}|\mathbf{q}|}. \tag{47}$$

To remove the dependence on Λ from F, we consider suitable values for ρ_0, for instance $\rho_0 > 5/\Lambda$, such that, as shown in Appendix B, we can rewrite F in terms of Bessel functions [25]:

$$F(\rho_0|\mathbf{q}|,\Lambda) \approx I_0(\rho_0|\mathbf{q}|)K_0(\rho_0|\mathbf{q}|) + I_1(\rho_0|\mathbf{q}|)K_1(\rho_0|\mathbf{q}|), \tag{48}$$

where I_ν and K_ν are the modified Bessel functions of first and second kind, respectively, and, hereafter, we write the function F as $F(\rho_0|\mathbf{q}|)$.

Finally, we consider the map $(\alpha, v_F) \to (\alpha^*_{\rho_0,\mathbf{q}}, v^*_{\rho_0,\mathbf{q}})$ in Eq. (32), rewriting Π_{2b} in terms of these renormalized parameters until $\mathcal{O}(\alpha^*_{\rho_0,\mathbf{q}})$, namely

$$\Pi_{2b}(\rho_0,\omega,\mathbf{q}) = \frac{e^2|\mathbf{q}|\alpha^*_{\rho_0,\mathbf{q}}}{v^*_{\rho_0,\mathbf{q}}}p_{2b}(\rho_0|\mathbf{q}|,y^*_{\rho_0,q}). \tag{49}$$

By inserting Eqs. (45) and (49) into (15), we can write the 00 component of the polarization tensor, corrected until 2-loop order, in terms of the renormalized parameters, namely

$$\Pi(\rho_0,\omega,\mathbf{q}) \approx -\frac{e^2|\mathbf{q}|}{4v^*_{\rho_0,\mathbf{q}}\sqrt{1-y^{*2}_{\rho_0,q}}} + \frac{e^2|\mathbf{q}|\alpha^*_{\rho_0,\mathbf{q}}}{v^*_{\rho_0,\mathbf{q}}} \times [p_{2a}(\rho_0|\mathbf{q}|,y^*_{\rho_0,q}) + p_{2b}(\rho_0|\mathbf{q}|,y^*_{\rho_0,q})]. \tag{50}$$

The pole in Eq. (50), at $x^*_{\rho_0,q} = 1$, determines a threshold from which ($x^*_{\rho_0,q} > 1$) the polarization tensor has a imaginary part, which is connected to the real part of the longitudinal conductivity. According to Ref. [44], for

the case without the presence of the conducting plate, it was argued that as $x_q^* \to 1$ the 2-loop results tend to be unreliable, since higher order corrections become as important as the 2-loop ones. In the present case, with the presence of the conducting plate, we expect a similar behavior, so that, as $x_{\rho_0,q}^* \to 1$, the 2-loop results become less reliable.

As an application of the above calculations, we determine the longitudinal conductivity and its optical limit.

V. THE CONDUCTIVITY

As shown in Appendix C, the longitudinal conductivity, $\sigma(\omega, \mathbf{q})$, can be obtained in terms of the 00-component of the polarization tensor $\Pi(\omega, \mathbf{q})$ as follows [27,44,46]:

$$\sigma(\omega, \mathbf{q}) = \frac{i\omega\Pi(\omega, \mathbf{q})}{|\mathbf{q}|^2}. \tag{51}$$

From Eqs. (50) and (51), the longitudinal conductivity becomes

$$\frac{\sigma(\rho_0, \omega, \mathbf{q})}{\sigma_0} \approx 4ix_{\rho_0,q}^* \left\{ -\frac{1}{4\sqrt{1 - y_{\rho_0,q}^{*2}}} + \alpha_{\rho_0,\mathbf{q}}^* \times [p_{2a}(\rho_0|\mathbf{q}|, y_{\rho_0,q}^*) + p_{2b}(\rho_0|\mathbf{q}|, y_{\rho_0,q}^*)] \right\}. \tag{52}$$

In order to visualize the results in terms of quantities that do not vary with ρ_0, we write $x_{\rho_0,q}^*$ as a function of x_q^*, which is done using Eqs. (7) and (14), remembering that $\alpha_{\mathbf{q}}^* = e^2/(\kappa v_{\mathbf{q}}^*)$, giving

$$x_{\rho_0,q}^* = \frac{x_q^*}{1 - \frac{\alpha_{\mathbf{q}}^*}{4} F(\rho_0|\mathbf{q}|)} \quad \text{and} \quad \alpha_{\rho_0,\mathbf{q}}^* = \frac{\alpha_{\mathbf{q}}^*}{1 - \frac{\alpha_{\mathbf{q}}^*}{4} F(\rho_0|\mathbf{q}|)}. \tag{53}$$

For further analysis, taking into account the real part of the longitudinal conductivity, it is convenient to define

$$\tilde{\sigma}_1(\rho_0|\mathbf{q}|, x_q^*) = -\mathrm{Re}\left\{ \frac{ix_q^*}{\sqrt{\left[1 - \frac{\alpha_{\mathbf{q}}^*}{4} F(\rho_0|\mathbf{q}|)\right]^2 - y_q^{*2}}} \right\}, \tag{54}$$

which is the real part of the ratio (52), calculated until 1-loop order of perturbation (the subscript 1 means that the formula takes into account calculations up to 1-loop). We also define:

$$\tilde{\sigma}_2(\rho_0|\mathbf{q}|, x_q^*) = \mathrm{Re}\left\{ -\frac{ix_q^*}{\sqrt{\left[1 - \frac{\alpha_{\mathbf{q}}^*}{4} F(\rho_0|\mathbf{q}|)\right]^2 - y_q^{*2}}} + \frac{4ix_q^*\alpha_{\mathbf{q}}^*}{\left[1 - \frac{\alpha_{\mathbf{q}}^*}{4} F(\rho_0|\mathbf{q}|)\right]^2} \left[p_{2a}\left(\rho_0|\mathbf{q}|, \frac{y_q^*}{1 - \frac{\alpha_{\mathbf{q}}^*}{4} F(\rho_0|\mathbf{q}|)}\right) + p_{2b}\left(\rho_0|\mathbf{q}|, \frac{y_q^*}{1 - \frac{\alpha_{\mathbf{q}}^*}{4} F(\rho_0|\mathbf{q}|)}\right) \right] \right\}, \tag{55}$$

which is the real part of the ratio (52), written in terms of x_q^* and $\alpha_{\mathbf{q}}^*$ using Eq. (53). The subscript 2 means we are going until 2-loop perturbation order.

In Fig. 4(a), we plotted the real part of the conductivity at 1-loop order, represented by $\tilde{\sigma}_1(\rho_0|\mathbf{q}|, x_q^*)$, given in Eq. (54). The three curves correspond to $\tilde{\sigma}_1(\rho_0|\mathbf{q}| \to \infty, x_q^*)$ (dashed line), $\tilde{\sigma}_1(\rho_0|\mathbf{q}| = 5, x_q^*)$ (dot-dashed line) and $\tilde{\sigma}_1(\rho_0|\mathbf{q}| = 1, x_q^*)$ (dotted line). From this panel we can take two conclusions: first, as we bring the conducting plate closer to the $2+1$D system, the 1-loop conductivity increases, with such effect being more noticeable as we approach the point $\omega/(v_{\mathbf{q}}^*|\mathbf{q}|) = 1$; second, for a fixed ρ_0, we also see an increase in the conductivity as $|\mathbf{q}|$ decreases, which is a consequence of the product $\rho_0|\mathbf{q}|$ in the exponential term of the photon propagator (10).

In Fig. 4(b), we plotted the real part of the conductivity up to 2-loop perturbation, represented by $\tilde{\sigma}_2(\rho_0|\mathbf{q}|, x_q^*)$, given by Eq. (55), and, for comparison, the 1-loop correction for $\rho_0|\mathbf{q}| = 1$, i.e., $\tilde{\sigma}_1(\rho_0|\mathbf{q}| = 1, x_q^*)$. The 2-loop curves correspond to $\tilde{\sigma}_2(\rho_0|\mathbf{q}| \to \infty, x_q^*)$ (long dashed line), $\tilde{\sigma}_2(\rho_0|\mathbf{q}| = 5, x_q^*)$ (dot-long-dashed line) and $\tilde{\sigma}_2(\rho_0|\mathbf{q}| = 1, x_q^*)$ (small dashed line). When the product $\rho_0|\mathbf{q}|$ decreases, we observe an inhibition of the 2-loop correction, which, therefore, causes a displacement of the longitudinal conductivity towards the 1-loop correction, leading to an increase in the conductivity even more evident than at 1-loop. In other words, as the distance between the conducting plate and the $2+1$D system gets smaller, the contribution of the 2-loop polarization diagrams becomes inhibited, and this leads to an enhancement of the conductivity for this part of the spectrum (in the optical limit we see a slightly different behavior). On the other hand, for a fixed ρ_0, if we vary $|\mathbf{q}|$ and ω such that the ratio $\omega/(v_{\mathbf{q}}^*|\mathbf{q}|)$ remains constant, the previous behavior will also be observed: a cancellation of the 2-loop corrections as $|\mathbf{q}|$ decreases, leading to an increase of $\tilde{\sigma}_2(\rho_0|\mathbf{q}|, x_q)$. We must

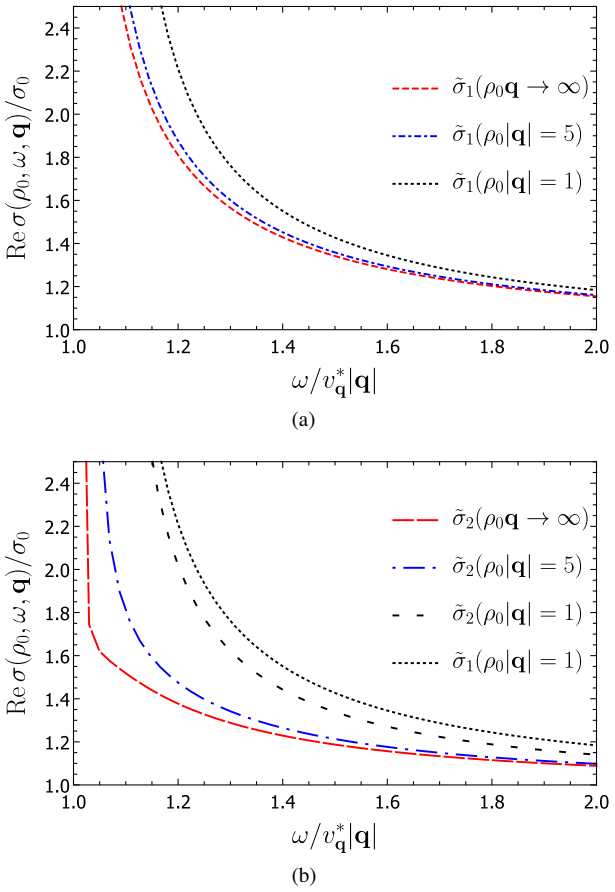

FIG. 4. (a) Representation of the real part of the conductivity at 1-loop perturbation order, where the dashed line accounts for $\tilde{\sigma}_1(\rho_0|\mathbf{q}|\to\infty, x_q^*)$, the dot-dashed line for $\tilde{\sigma}_1(\rho_0|\mathbf{q}|=5, x_q^*)$ and the dotted line for $\tilde{\sigma}_1(\rho_0|\mathbf{q}|=1, x_q^*)$. (b) Presentation of the curves for the longitudinal conductivity up to 2-loop perturbation order, where the long-dashed line accounts for $\tilde{\sigma}_2(\rho_0|\mathbf{q}|\to\infty, x_q^*)$, the dot-long-dashed line for $\tilde{\sigma}_2(\rho_0|\mathbf{q}|=5, x_q^*)$ and the small dashed line for $\tilde{\sigma}_2(\rho_0|\mathbf{q}|=1, x_q^*)$, we also plotted $\tilde{\sigma}_1(\rho_0|\mathbf{q}|=1, x_q^*)$ for comparison purposes. Both panels have $\omega/(v_{\mathbf{q}}^*|\mathbf{q}|)$ as the horizontal axis. We made $\alpha_{\mathbf{q}}^*=0.3$ as in Ref. [44].

highlight that this feature is not observed in graphene in the absence of the plate [47], since the only dependence it has on the external momentum comes from $\omega/(v_{\mathbf{q}}^*|\mathbf{q}|)$, but varying $|\mathbf{q}|$ while keeping this quantity constant will not affect the conductivity.

A. The optical limit

In Ref. [26], the authors considered the real part of the optical conductivity $\sigma_{\mathrm{opt}}(\omega)$ as presented in Ref. [48],

$$\frac{\mathrm{Re}[\sigma_{\mathrm{opt}}^*(\omega)]}{\sigma_0}=1+C\alpha_{\omega/v_F}^*\equiv 1+C\alpha\frac{v_F}{v_{\mathbf{q}}^*}\bigg|_{|\mathbf{q}|=\omega/v_F}, \tag{56}$$

where C is a constant, $\sigma_0=e^2/4$ is the minimal conductivity of graphene and the superscript in σ^* sets the dependence on the renormalized parameter α_{ω/v_F}^*. In Ref. [26], it is suggested that the optical conductivity should increase due to the inhibition of the renormalization of the Fermi velocity by the conducting surface. In order to verify this proposal, we compute the optical conductivity from the following limit [47]:

$$\sigma_{\mathrm{opt}}(\rho_0,\omega)=\lim_{|\mathbf{q}|\to 0}\frac{i\omega}{|\mathbf{q}|^2}\Pi(\rho_0,\omega,\mathbf{q}). \tag{57}$$

From the above definition, we show, in Appendix D, that the optical conductivity is given by

$$\tilde{\sigma}_{\mathrm{opt}}(\rho_0,\omega)=\frac{\mathrm{Re}[\sigma_{\mathrm{opt}}(\rho_0,\omega)]}{\sigma_0}\approx 1+C(\rho_0\omega/v_F)\alpha, \tag{58}$$

where

$$\begin{aligned}C(\rho_0\omega/v_F)=C_0&+\frac{\rho_0\omega}{8v_F}\frac{d}{d(\rho_0|\mathbf{k}|)}F(\rho_0|\mathbf{k}|)\bigg|_{|\mathbf{k}|=\omega/2v_F}\\&+\int_0^\pi\frac{d\theta}{\pi}\int_0^\infty du\frac{\cos\theta(u+\cos\theta)}{(1-u^2)\sqrt{u^2+1-2u\cos\theta}}\\&\times\exp\left(-\frac{\rho_0\omega}{v_F}\sqrt{u^2+1-2u\cos\theta}\right),\end{aligned} \tag{59}$$

and

$$C_0=\frac{19-6\pi}{12}\approx 0.0125 \tag{60}$$

is the 2-loop term calculated in Ref. [47].

In the context of graphene with no plate [39,47], one makes $\alpha\to\alpha_{\omega/(2v_F)}^*$, therefore, considering the existence of the plate, we must make $\alpha\to\alpha_{\rho_0,\omega/(2v_F)}^*$, obtaining:

$$\frac{\mathrm{Re}[\sigma_{\mathrm{opt}}^*(\rho_0,\omega)]}{\sigma_0}=1+C(\rho_0\omega/v_F)\alpha_{\rho_0,\omega/v_F}^*, \tag{61}$$

which is correspondent to Eq. (56). Therefore, the above equation is the proper description of the optical conductivity of graphene in the presence of a conducting surface, computing the new C factor and not just considering $v_{\mathbf{q}}^*\to v_{\rho_0,\mathbf{q}}^*$ in Eq. (56), as supposed in Ref. [26].

In Fig. 5(a), we plot the real part of the optical conductivity as a function of $\rho_0\omega/v_F$, where the solid line corresponds to Eq. (61). In this figure, the point P_1 is where the optical conductivity is equal to the minimal conductivity (represented by the dotted line), which means a total cancellation of the 2-loop correction due to the presence of the plate in the limit $\rho_0\to 0$. The point P_2 is where the optical conductivity in the presence of the plate equals the optical conductivity without the plate (dashed line). The point P_3 represents the peak of conductivity. Then, as the distance ρ_0 gets bigger, the optical conductivity tends to the case without the plate, as expected.

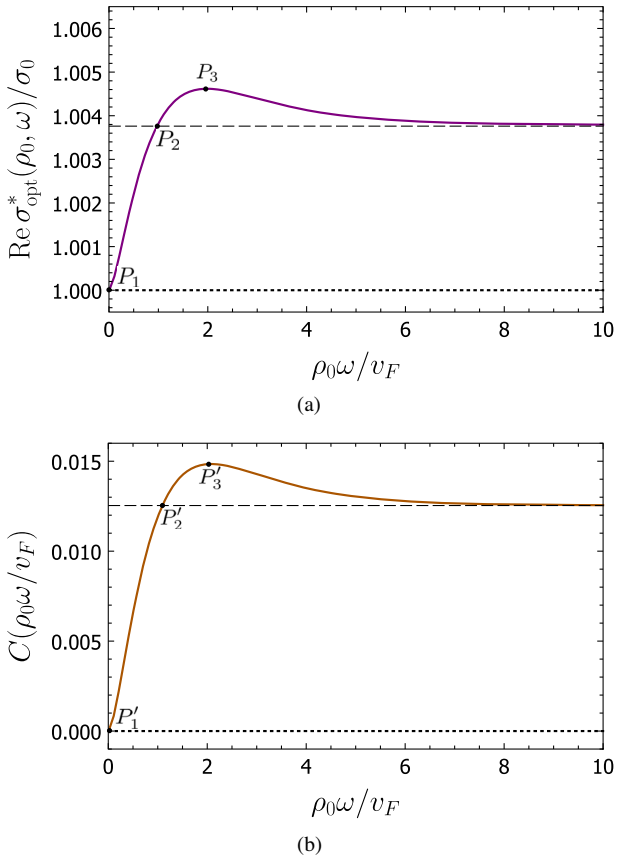

FIG. 5. (a) The solid line corresponds to the real part of the optical conductivity [Eq. (61)] for $\alpha^*_{\omega/v_F} = 0.3$. The dashed line represents the optical conductivity calculated until 2-loop order, without the presence of the plate. The dotted line corresponds to the minimal conductivity, given by the point P_1. P_2 is the point where the values, with or without plate, are the same. P_3 represents the maximum value of the optical conductivity. (b) The solid line corresponds to $C(\rho_0\omega/v_F)$ [Eq. (59)]. The dashed line represents $C_0 \approx 0.01$, and the dotted line serves as a reference for $C(\rho_0\omega/v_F) \approx 0$. At the point P'_3, $C(\rho_0\omega/v_F)$ reaches a maximum value, while at the point P'_2 we have $C(\rho_0\omega/v_F) = C_0$. At the point P'_1, $C(\rho_0\omega/v_F)$ becomes null.

In Fig. 5(b), the solid line corresponds to the function $C(\rho_0\omega/v_F)$, given by Eq. (59). At the limit $\rho_0 \to 0$, $C(\rho_0\omega/v_F)$ tends to zero, which is represented by the point P'_1, and whose value is indicated by the dotted line. As we increase the distance ρ_0, we get to the point P'_2, where $C(\rho_0\omega/v_F)$ coincides with $C_0 \approx 0.01$ (represented by the dashed line). As the distance ρ_0 becomes larger, the function $C(\rho_0\omega/v_F)$ increases until reaching a maximum value, given by the point P'_3. For $\rho_0 \to \infty$, we recover the C_0 obtained in Ref. [47], which is represented by the dashed line.

VI. ANALYSIS OF THE RESULTS AND FINAL COMMENTS

In the present paper, using PQED as the theory which describes the interactions of electrons in a $2+1$D system of massless Dirac fermions, we computed the 00-component of the photon self-energy, until 2-loop perturbation order and in the presence of a grounded perfectly conducting surface. As an application of our results, using the Kubo formula [Eq. (51)], we were able to determine the longitudinal and optical conductivities of the $2+1$D system. In the language of condensed matter, the $2+1$D system investigated by us is the representation of graphene in the low energy regime, since, in this approach, the dispersion relation of graphene is given by $E_\pm \approx \pm v_F|\mathbf{k}|$, where v_F is the Fermi velocity and $\mathbf{k}$ is the external momentum.

In our work, an important result is that the real part of the longitudinal conductivity increases when the distance between the $2+1$D system and the plate decreases. In Fig. 4(a), we see this enhancement for the 1-loop approximation [Eq. (54)], but it is more evident if we go up to 2-loop perturbation order [Eq. (55)], specifically near the point $\omega/(v^*_{\mathbf{q}}|\mathbf{q}|) = 1$, as shown in Fig. 4(b).

The longitudinal conductivity, obtained here for any frequency and momentum [Eq. (52)], leads, in the limit $|\mathbf{q}| \to 0$, to the optical conductivity [Eq. (57)]. In Ref. [26], considering Eq. (56), it is suggested that the optical conductivity of a graphene sheet near a conducting plate is increased (if compared to the case without the plate) due to the inhibition of the renormalization of the Fermi velocity by the plate. However, the authors didn't consider the influence of the plate on the C factor of Eq. (56). The calculations up to 2-loop perturbation order provide the correct C for the model, given by Eq. (59) and shown in Fig. 5(b). According to our results, even if we write the conductivity in terms of the bare parameters [as shown in Eq. (58)], the presence of the conducting plate generates a dependence on the frequency, what does not happen in the situation without the plate.

Therefore, considering contributions from both the C factor and the renormalization of the Fermi velocity, we obtain a proper description of the optical conductivity [Eq. (61)], presented in Fig. 5(a) as the solid line. In this panel, when the plate is infinitely distant from the $2+1$D system, we recover the result for the optical conductivity found in the literature [47], which is indicated by the dashed line in Fig. 5(a). As we bring the conducting plate closer to the $2+1$D system, the optical conductivity is increased (if compared to the case without the presence of a conducting plate), reaching a maximum value. After that, the optical conductivity decreases until it gets totally canceled in the limit of no distance between the conducting surface and the $2+1$D system.

In summary, our results give a theoretical description of the longitudinal and optical conductivities of a $2+1$D system, which is correlated to graphene, in the presence of a conducting plate. With calculations taken until 2-loop perturbation order, we showed that the longitudinal conductivity increases as we bring the conducting surface

closer to the $2+1$D system. In the optical limit, the conductivity can increase or decrease, depending on the position of the conducting plate. These results may be useful as an alternative way to control the longitudinal and optical conductivities of graphene.

ACKNOWLEDGMENTS

The authors thank N. M. R. Peres, E. C. Marino, A. N. Braga, J. D. L. Silva, E. Granhen, W. Pires and L. Fernández for fruitful discussions. D. C. P. was supported by Coordenação de Aperfeiçoamento de Pessoal de Nível Superior (CAPES/Brazil)—Processes No. 88882.445192/2018-01 and No. 88881.187657/2018-01. D. T. A. was supported by UFPA via Licença Capacitação (Portaria 5603/2019), and thanks the hospitality of the University of Minho (Portugal), as well as that of the International Iberian Nanotechnology Laboratory (INL-Portugal). V. S. A. is partially supported by Conselho Nacional de Desenvolvimento Científico e Tecnlógico (CNPq) and by CAPES/NUFFIC, finance code 0112.

APPENDIX A: THE SOKHOTSKI-PLEMELJ IDENTITY

Usually, the Sokhotski-Plemelj identity is presented as [45]

$$\lim_{\epsilon\to 0}\int_a^b \frac{f(x)}{x-x_0\pm i\epsilon}dx = P\int_a^b \frac{f(x)}{x-x_0}dx \mp i\pi f(x_0), \tag{A1}$$

where P is the Cauchy principal value. One can extend its definition to calculate integrals with higher order poles [45],

$$\lim_{\epsilon\to 0}\int_a^b \frac{f(x)}{(x-x_0\pm i\epsilon)^{n+1}}dx = \#\int_a^b \frac{f(x)}{(x-x_0)^{n+1}}dx, \mp i\pi\frac{f^{(n)}(x_0)}{n!}, \tag{A2}$$

where # represents the Hadamard finite-part integral (an extension of the Cauchy principal value integral), and is defined as

$$\#\int_a^b \frac{f(x)}{(x-x_0)^{n+1}}dx = \lim_{\epsilon\to 0}\left[\int_a^{x_0-\epsilon}\frac{f(x)}{(x-x_0)^{n+1}} + \int_{x_0+\epsilon}^b \frac{f(x)}{(x-x_0)^{n+1}} - H_n(x_0,\epsilon)\right], \tag{A3}$$

where

$$H_0 = 0, \tag{A4}$$

and

$$H_n = \sum_{k=0}^{n-1}\frac{h^{(k)}(x_0)}{k!(n-k)}\frac{(1-(-1)^{n-k})}{\epsilon^{n-k}}, \quad n=1,2,\ldots. \tag{A5}$$

Hereafter, we use the above representations to compute the real and imaginary parts of the 2-loop corrections to the polarization tensor for $x_q = \omega/(v_F|\mathbf{q}|) > 1$.

1. Π_{2a} diagram

First, we compute the real and imaginary parts of the integral $I_{a''}$ [Eq. (24)] of the Π_{2a} diagram, for $x_q > 1$.

a. Real part

Lets make a change of variables in Eq. (24),

$$w = \cosh\mu, \qquad d\mu = \frac{dw}{\sqrt{w^2-1}}, \tag{A6}$$

obtaining

$$I_{a''}(\rho_0|\mathbf{q}|, y_q) = \int_0^{2\pi} d\nu \int_1^\infty dw \frac{H(w,y_q,\nu)}{(w-y_q)^2}, \tag{A7}$$

where

$$H(w,y_q,\nu) = \frac{1}{\pi}\frac{\sin^2\nu(w-\cos\nu)(w^2+y_q^2)}{(w+y_q)^2\sqrt{w^2-1}} \times F\left(\frac{\rho_0|\mathbf{q}|}{2}(w-\cos\nu),\Lambda\right). \tag{A8}$$

Then, from Eqs. (A3) and (A5), we find the real part is given by

$$\mathrm{Re}[I_{a''}(\rho_0|\mathbf{q}|,x_q)] = \lim_{\epsilon\to 0^+}\left[\int_1^{x_q-\epsilon}\frac{H(w,x_q,\nu)}{(w-x_q)^2}dw + \int_{x_q+\epsilon}^\infty \frac{H(w,x_q,\nu)}{(w-x_q)^2}dw - \frac{2H(x_q,x_q,\nu)}{\epsilon}\right]. \tag{A9}$$

b. Imaginary part

From Eq. (A2), we obtain the imaginary part:

$$\mathrm{Im}[I_{a''}(\rho_0|\mathbf{q}|,x_q)] = \int_0^{2\pi} d\nu \left.\frac{dH(w,x_q,\nu)}{dw}\right|_{w=x_q}, \tag{A10}$$

where

$$\left.\frac{dH(w,x_q,\nu)}{dw}\right|_{w=x_q} = \frac{\sin^2\nu}{2\pi(x_q^2-1)^{3/2}}\left[(x_q\cos\nu-1)F\left(\frac{\rho_0|\mathbf{q}|}{2}(x_q-\cos\nu),\Lambda\right)\right.$$
$$\left.+(x_q^2-1)(x_q-\cos\nu)\frac{d}{dw}F\left(\frac{\rho_0|\mathbf{q}|}{2}(w-\cos\nu),\Lambda\right)\right|_{w=x_q}\Bigg]. \quad \text{(A11)}$$

2. Π_{2b} diagram

Here, we compute the real and imaginary parts of the Π_{2b} correction to the vacuum polarization, represented by Eq. (33). In the following steps, our calculations are similar to Ref. [44], though leading to different representations, they generate the same numerical results.

Since Eq. (33) has a first order pole, we can apply the usual definition of the Sokhotski-Plemelj identity, but in terms of the delta function [44]:

$$\frac{1}{x-x_0\pm i\epsilon} = P\frac{1}{x-x_0}\mp i\pi\delta(x-x_0), \quad \text{(A12)}$$

which can be also generalized for a function on the denominator,

$$\frac{1}{g(x)\pm i\epsilon} = \sum_i\left[P\frac{1}{g(x_i)}\mp i\pi\delta(g(x_i))\right], \quad \text{(A13)}$$

where $g(x)$ is an invertible function in the region of integration, and the δ function of a function is given by [49]

$$\delta(g(x)) = \sum_i\frac{\delta(x-x_i)}{|g'(x_i)|}, \quad \text{(A14)}$$

assuming $x=x_i$ are the zeros of $g(x)$.

In Eq. (33), making $x_q=\cosh(\lambda/2)$ [44], we must define two functions in the denominator, namely

$$g_+(a,b,\lambda) = \cosh(a+b)-\cosh\lambda, \quad \text{(A15)}$$

and

$$g_-(a,b,\lambda) = \cosh(a-b)-\cosh\lambda, \quad \text{(A16)}$$

which have poles at $a_\pm=\lambda\mp b$. Hence, Eq. (33) leads to

$$p_{2b}(\rho_0|\mathbf{q}|,x_q) = -\frac{1}{16\pi^3}\int_0^\infty db\int_b^\infty da \times\frac{U(a,b,\rho_0|\mathbf{q}|,\lambda(x_q))}{[g_+(a,b,\lambda(x_q))-i\epsilon][g_-(a,b,\lambda(x_q))-i\epsilon]}, \quad \text{(A17)}$$

where

$$U(a,b,\rho_0|\mathbf{q}|,\lambda) = (\cosh^2 a-\cosh^2 b)M_1(a,b,\rho_0|\mathbf{q}|)+\left(\frac{\cosh\lambda+3}{2}\right)(\cosh a+\cosh b)M_2(a,b,\rho_0|\mathbf{q}|)$$
$$+\frac{\cosh\lambda+1}{2}(\cosh a-\cosh b)M_3(a,b,\rho_0|\mathbf{q}|). \quad \text{(A18)}$$

Next, we explicit the real and imaginary parts of p_{2b}.

a. Real part

As mentioned before, the real part of p_{2b} will be calculated by taking the principal value of (A17), namely

$$\mathrm{Re}[p_{2b}(\rho_0|\mathbf{q}|,x_q)] = -\frac{1}{16\pi^3}\lim_{\epsilon\to0^+}\int_0^\infty db\left[\int_b^{\lambda(x_q)-b-\epsilon}da\frac{U(a,b,\rho_0|\mathbf{q}|,\lambda(x_q))}{g_+(a,b,\lambda(x_q))g_-(a,b,\lambda(x_q))}\right.$$
$$\left.+\int_{\lambda(x_q)-b+\epsilon}^{\lambda(x_q)+b-\epsilon}da\frac{U(a,b,\rho_0|\mathbf{q}|,\lambda(x_q))}{g_+(a,b,\lambda(x_q))g_-(a,b,\lambda(x_q))}+\int_{\lambda(x_q)+b+\epsilon}^\infty da\frac{U(a,b,\rho_0|\mathbf{q}|,\lambda(x_q))}{g_+(a,b,\lambda(x_q))g_-(a,b,\lambda(x_q))}\right]. \quad \text{(A19)}$$

b. Imaginary part

The poles of the functions $g_+(a,b,\lambda)$ and $g_-(a,b,\lambda)$ are not the same. Therefore, we have

$$\delta(g_+(a,b,\lambda)) = \frac{\delta(a-(\lambda-b))}{\sinh\lambda} \quad \text{and} \quad \delta(g_-(a,b,\lambda)) = \frac{\delta(a-(\lambda+b))}{\sinh\lambda}. \tag{A20}$$

Hence, the imaginary part of Eq. (A17) becomes

$$\mathrm{Im}[p_{2b}(\rho_0|\mathbf{q}|,x_q)] = -\frac{1}{32\pi^2\sinh\lambda(x_q)}\left\{\int_0^{\lambda(x_q)/2}\frac{db}{\sinh b}\left[\frac{U(\lambda(x_q)+b,b,\lambda(x_q))}{\sinh(b+\lambda(x_q))}-\frac{U(\lambda(x_q)-b,b,\lambda(x_q))}{\sinh(\lambda(x_q)-b)}\right]\right.$$
$$\left.+\int_{\lambda(x_q)/2}^{\infty}\frac{db}{\sinh b}\frac{U(\lambda(x_q)+b,b,\lambda(x_q))}{\sinh(b+\lambda(x_q))}\right\}. \tag{A21}$$

APPENDIX B: THE $F(\rho_0|\mathbf{q}|)$ APPROXIMATION

The integral in Eq. (12) has a cutoff at ξ_Λ, which is given in terms of the momentum cutoff Λ by Eq. (13). As explained in Ref. [25], the integrand of (12) can vanish before reaching the cutoff ξ_Λ. In Figs. 6(a) and 6(b) we plot the integrand of Eq. (13), and also the cutoff ξ_Λ, represented by the solid line. In Fig. 6(a) ($\rho_0 = 1/\Lambda$), we observe that the integrand is not null at $\xi = \xi_\Lambda$. On the other hand, in Fig. 6(b) ($\rho_0 = 5/\Lambda$), the integrand vanishes before reaching the cutoff ξ_Λ. Therefore, choosing the appropriate ρ_0, for instance $\rho_0 > 5/\Lambda$, the integral in ξ tends to

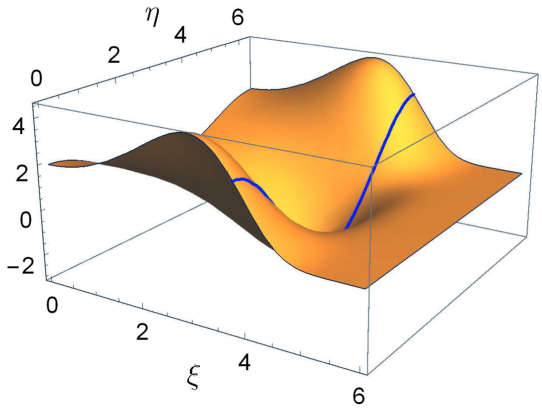

(a) Integrand of F for $\rho_0 = 1/\Lambda$.

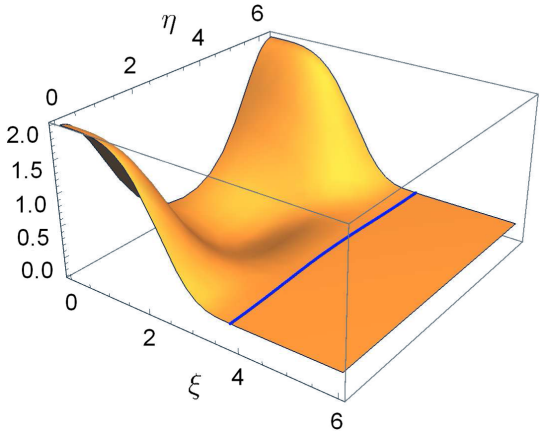

(b) Integrand of F for $\rho_0 = 5/\Lambda$.

FIG. 6. In (a) and (b) we plot the integrand of F [Eq. (12)] for $\rho_0 = 1/\Lambda$ and $\rho_0 = 1/\Lambda$, respectively, with $|\mathbf{q}| = \Lambda/10$. The solid line corresponds to the cutoff ξ_Λ.

$$\int_0^{\xi_\Lambda} d\xi \to \int_0^{\infty} d\xi, \tag{B1}$$

and, the function F can be rewritten as [25]

$$F(\rho_0|\mathbf{q}|,\Lambda) \approx I_0(\rho_0|\mathbf{q}|)K_0(\rho_0|\mathbf{q}|) + I_1(\rho_0|\mathbf{q}|)K_1(\rho_0|\mathbf{q}|), \tag{B2}$$

where I_μ and K_ν are the modified Bessel functions of first and second kind, respectively.

APPENDIX C: THE RELATION BETWEEN THE LONGITUDINAL CONDUCTIVITY AND Π_{00}

From the Kubo formula [27] we get the definition of the conductivity in terms of the polarization tensor, namely

$$\sigma^{ij}(\omega,\mathbf{q}) = \frac{i}{\omega}\Pi^{ij}(\omega,\mathbf{q}). \tag{C1}$$

The spatial components Π^{ij} can be written as [50]

$$\Pi^{ij}(\omega,\mathbf{q}) = \Pi^L(\omega,|\mathbf{q}|)\frac{q^iq^j}{|\mathbf{q}|^2} + \Pi^T(\omega,|\mathbf{q}|)\left(\delta^{ij}-\frac{q^iq^j}{|\mathbf{q}|^2}\right), \tag{C2}$$

where Π_L and Π_T are the longitudinal and transverse components of the polarization tensor, which leads to a definition of the longitudinal and transverse conductivities. In the present paper, we are interested in the longitudinal part, given by

$$\sigma_L(\omega,|\mathbf{q}|)=\frac{i}{\omega}\Pi_L(\omega,|\mathbf{q}|). \tag{C3}$$

In order to isolate the longitudinal component, we multiply both sides of Eq. (C2) by q_iq_j and sum over, obtaining that

$$q_iq_j\Pi^{ij}(\omega,\mathbf{q})=|\mathbf{q}|^2\Pi^L(\omega,|\mathbf{q}|). \tag{C4}$$

From the continuity equation, given by [50]

$$\partial_\mu J^\mu=0, \tag{C5}$$

where $J^\mu=(\rho,\mathbf{J})$ is the quadricurrent, one can also show that [50]

$$\frac{q_iq_j}{\omega^2}\Pi^{ij}(\omega,\mathbf{q})=\Pi^{00}(\omega,|\mathbf{q}|), \tag{C6}$$

which, combined with Eq. (C4), leads to

$$\Pi^{00}(\omega,|\mathbf{q}|)=\frac{|\mathbf{q}|^2}{\omega^2}\Pi^L(\omega,|\mathbf{q}|). \tag{C7}$$

Therefore, by replacing the above equation into Eq. (C1), the longitudinal conductivity can be given in terms of the 00-component of the polarization tensor as

$$\sigma(\omega,|\mathbf{q}|)=i\frac{\omega}{|\mathbf{q}|^2}\Pi^{00}(\omega,|\mathbf{q}|), \tag{C8}$$

where $\sigma_L(\omega,|\mathbf{q}|)$ was replaced by $\sigma(\omega,|\mathbf{q}|)$ throughout the text.

APPENDIX D: THE OPTICAL LIMIT

The optical conductivity can be represented as

$$\sigma_{\rm opt}(\rho_0,\omega)\approx\sigma_{\rm opt,1}(\omega)+\sigma_{\rm opt,2a}(\rho_0,\omega)+\sigma_{\rm opt,2b}(\rho_0,\omega), \tag{D1}$$

where

$$\sigma_{\rm opt,1}(\omega)=\lim_{|\mathbf{q}|\to0}\frac{i\omega}{|\mathbf{q}|^2}\Pi_1(\omega,\mathbf{q}), \tag{D2}$$

$$\sigma_{\rm opt,2a}(\rho_0,\omega)=\lim_{|\mathbf{q}|\to0}\frac{i\omega}{|\mathbf{q}|^2}2\Pi_{2a}(\rho_0,\omega,\mathbf{q}), \tag{D3}$$

$$\sigma_{\rm opt,2b}(\rho_0,\omega)=\lim_{|\mathbf{q}|\to0}\frac{i\omega}{|\mathbf{q}|^2}\Pi_{2b}(\rho_0,\omega,\mathbf{q}). \tag{D4}$$

From Eq. (16), we get that $\sigma_{\rm opt,1}(\omega)$ will be given by

$$\sigma_{\rm opt,1}(\omega)=\lim_{|\mathbf{q}|\to0}\frac{i\omega}{|\mathbf{q}|^2}\Pi_1(\omega,\mathbf{q})=\frac{e^2}{4}=\sigma_0, \tag{D5}$$

so that the contribution of $\sigma_{\rm opt,1}$ results in the minimal conductivity σ_0.

Obtaining $\sigma_{\rm opt,2a}(\omega)$ requires the calculation Π_{2a} in Eq. (D3). Using Eq. (19), we have

$$\begin{aligned}\Pi_{2a}(\rho_0,\omega,\mathbf{q})=&-\frac{Ne^4}{2\kappa}\int\frac{d^2k}{(2\pi)^2}\frac{\mathbf{k}\cdot(\mathbf{k}+\mathbf{q})-|\mathbf{k}||\mathbf{k}+\mathbf{q}|}{|\mathbf{k}+\mathbf{q}|}\\&\times\frac{[v_F^2(|\mathbf{k}|+|\mathbf{k}+\mathbf{q}|)^2+\omega^2]}{[v_F^2(|\mathbf{k}|+|\mathbf{k}+\mathbf{q}|)^2-\omega^2]^2}\\&\times[\ln(\Lambda/|\mathbf{k}|)-F(\rho_0|\mathbf{k}|)],\end{aligned} \tag{D6}$$

where we made $\mathbf{k}\to-\mathbf{k}-\mathbf{q}$. Expanding until order $|\mathbf{q}|^2$ leads to

$$\begin{aligned}\Pi_{2a}(\rho_0,\omega,\mathbf{q})=&-\frac{Ne^4}{2\kappa}\int\frac{d^2k}{(2\pi)^2}\frac{\frac{1}{2}|\mathbf{q}|^2(\cos^2\theta-1)}{|\mathbf{k}|}\\&\times\left(\frac{4v_F^2|\mathbf{k}|^2-q_0^2}{4v_F^2|\mathbf{k}|^2+q_0^2}\right)[\ln(\Lambda/|\mathbf{k}|)-F(\rho_0|\mathbf{k}|)],\end{aligned} \tag{D7}$$

where θ is the angle between $\mathbf{k}$ and $\mathbf{q}$. Then, integrating in the polar coordinate system, we get

$$\begin{aligned}\Pi_{2a}(\rho_0,\omega,\mathbf{q})=&\frac{e^2|\mathbf{q}|^2v_F\alpha}{8\pi}\int d|\mathbf{k}|\frac{(4v_F^2|\mathbf{k}|^2+\omega^2)}{(4v_F^2|\mathbf{k}|^2-\omega^2)^2}\\&\times\left[\ln\left(\frac{\Lambda}{|\mathbf{k}|}\right)-F(\rho_0|\mathbf{k}|)\right].\end{aligned} \tag{D8}$$

The above integral has a second order pole, and its imaginary part will be obtained from the following formula, better explained in Appendix A:

$$\mathrm{Im}\left\{\lim_{\epsilon\to0}\int_a^b\frac{f(x)}{(x-x_0\pm i\epsilon)^{n+1}}dx\right\}=\mp\pi\frac{f^{(n)}(x_0)}{n!}. \tag{D9}$$

In our case, $n=1$ and we define

$$f(|\mathbf{k}|)=\frac{(4v_F^2|\mathbf{k}|^2+\omega^2)[\ln(\frac{\Lambda}{|\mathbf{k}|})-F(\rho_0|\mathbf{k}|)]}{(2v_F|\mathbf{k}|+\omega)^2}, \tag{D10}$$

with derivative given by

$$\frac{df}{d|\mathbf{k}|}=-\frac{v_F}{\omega}-\frac{\rho_0}{2}\frac{dF(\rho_0|\mathbf{k}|)}{d(\rho_0|\mathbf{k}|)}\bigg|_{|\mathbf{k}|=\omega/2v_F}. \tag{D11}$$

Therefore, we have that

$$\begin{aligned}\mathrm{Im}[2\Pi_{2a}(\rho_0,\omega,\mathbf{q})]=&-\frac{e^2}{4}\frac{|\mathbf{q}|^2}{\omega}\frac{\alpha}{4}\left(1+\frac{\rho_0\omega}{v_F}\frac{1}{2}\right.\\&\left.\times\frac{dF(\rho_0|\mathbf{k}|)}{d(\rho_0|\mathbf{k}|)}\bigg|_{|\mathbf{k}|=\omega/2v_F}\right).\end{aligned} \tag{D12}$$

Hence, from (D3), the above contribution to the real part of the conductivity will be

$$\mathrm{Re}[\sigma_{\mathrm{opt},2a}(\rho_0,\omega)] = \frac{\sigma_0\alpha}{4}\left(1+\frac{\rho_0\omega}{2v_F}\frac{dF(\rho_0|\mathbf{k}|)}{d(\rho_0|\mathbf{k}|)}\bigg|_{|\mathbf{k}|=\frac{\omega}{2v_F}}\right), \tag{D13}$$

where the first term was obtained in [47].

The $\sigma_{\mathrm{opt},2b}(\omega)$ contribution is given by Eq. (D4). Expanding the Π_{2b} contribution until order $|\mathbf{q}|^2$ in Eq. (30), it follows that:

$$\begin{aligned}\Pi_{2b}(\rho_0,\omega,\mathbf{q}) = &-\frac{Ne^4|\mathbf{q}|^2}{2\kappa(2\pi)^3}\int_0^\infty d|\mathbf{k}|\int_0^\infty d|\mathbf{p}|\int_0^{2\pi}d\theta_k \\ &\times\int_0^{2\pi}d\theta_p|\mathbf{k}||\mathbf{p}|[\cos(\theta_k-\theta_p)-\cos(\theta_k+\theta_p)] \\ &\times\frac{[\frac{\omega^2}{|\mathbf{k}||\mathbf{p}|}\cos(\theta_k-\theta_p)+4v_F^2](1-e^{-2\rho_0|\mathbf{k}-\mathbf{p}|})}{|\mathbf{k}-\mathbf{p}|(4v_F^2|\mathbf{k}|^2-\omega^2)(4v_F^2|\mathbf{p}|^2-\omega^2)},\end{aligned} \tag{D14}$$

where we have made $\mathbf{q}=(|\mathbf{q}|,0)$ such that $\theta_{kq}=\theta_k$ and $\theta_{pq}=\theta_p$. From a change of variables, $\theta=\theta_k-\theta_p$ and $\varphi=\theta_k+\theta_p$, one can easily obtain that

$$\begin{aligned}\Pi_{2b}(\rho_0,\omega,\mathbf{q}) = &-\frac{e^4}{2\pi\kappa}|\mathbf{q}|^2\int_0^\pi\frac{d\theta}{\pi}\int_0^\infty d|\mathbf{k}|\int_0^\infty d|\mathbf{p}||\mathbf{k}| \\ &\times\frac{|\mathbf{p}|\cos\theta(\frac{\omega^2}{|\mathbf{k}||\mathbf{p}|}\cos\theta+4v_F^2)}{(4v_F^2|\mathbf{k}|^2-\omega^2)(4v_F^2|\mathbf{p}|^2-\omega^2)} \\ &\times\frac{\left(1-e^{-2\rho_0\sqrt{|\mathbf{k}|^2+|\mathbf{p}|^2-2|\mathbf{k}||\mathbf{p}|\cos\theta}}\right)}{\sqrt{|\mathbf{k}|^2+|\mathbf{p}|^2-2|\mathbf{k}||\mathbf{p}|\cos\theta}}.\end{aligned} \tag{D15}$$

From Eq. (A13), we find that the imaginary part of the above equation will be given in terms of

$$\mathrm{Im}\left[\frac{1}{4v_F^2|\mathbf{p}|^2-\omega^2}\right] = \frac{\pi}{4\omega v_F}\delta(|\mathbf{p}|-\omega/2v_F), \tag{D16}$$

and

$$\mathrm{Im}\left[\frac{1}{4v_F^2|\mathbf{k}|^2-\omega^2}\right] = \frac{\pi}{4\omega v_F}\delta(|\mathbf{k}|-\omega/2v_F). \tag{D17}$$

Due to symmetry, we can multiply the integral in (D15) by 2 and consider only the imaginary part of $\mathbf{p}$, giving ($u=2v_F|\mathbf{k}|/\omega$)

$$\begin{aligned}\mathrm{Im}[\Pi_{2b}(\rho_0,\omega,\mathbf{q})] = &\frac{\sigma_0|\mathbf{q}|^2\alpha}{\omega}\int_0^\pi\frac{d\theta}{\pi}\int_0^\infty du\frac{(u+\cos\theta)}{(1-u^2)} \\ &\times\frac{\cos\theta[1-\exp(-\frac{\rho_0\omega}{v_F}\sqrt{u^2+1-2u\cos\theta})]}{\sqrt{u^2+1-2u\cos\theta}},\end{aligned} \tag{D18}$$

where the first term in the integral was determined in [47], giving

$$\begin{aligned}&\mathrm{Re}[\sigma_{\mathrm{opt},2b}(\rho_0,\omega)] \\ &= \sigma_0\alpha\left[\frac{8-3\pi}{6}+\int_0^\pi\frac{d\theta}{\pi}\int_0^\infty du\right. \\ &\left.\times\frac{\cos\theta(u+\cos\theta)\exp(-\frac{\rho_0\omega}{v_F}\sqrt{u^2+1-2u\cos\theta})}{(1-u^2)\sqrt{u^2+1-2u\cos\theta}}\right].\end{aligned} \tag{D19}$$

Therefore, from Eqs. (D13) and (D19) we obtain

$$\tilde{\sigma}_{\mathrm{opt}}(\rho_0,\omega) = \frac{\mathrm{Re}[\sigma_{\mathrm{opt}}(\rho_0,\omega)]}{\sigma_0} \approx 1 + C(\rho_0\omega/v_F)\alpha \tag{D20}$$

where

$$\begin{aligned}C(\rho_0\omega/v_F) = &\,C_0+\frac{\rho_0\omega}{8v_F}\frac{d}{d(\rho_0|\mathbf{k}|)}F(\rho_0|\mathbf{k}|)\bigg|_{|\mathbf{k}|=\omega/2v_F} \\ &+\int_0^\pi\frac{d\theta}{\pi}\int_0^\infty du\frac{\cos\theta(u+\cos\theta)}{(1-u^2)\sqrt{u^2+1-2u\cos\theta}} \\ &\times\exp\left(-\frac{\rho_0\omega}{v_F}\sqrt{u^2+1-2u\cos\theta}\right),\end{aligned} \tag{D21}$$

and $C_0=\frac{19-6\pi}{12}\approx 0.0125$ [47].

[1] S. Girvin and R. Prange, *The Quantum Hall Effect* (Springer, New York, 1987).

[2] F. Wilczek, *Fractional Statistics and Anyon Superconductivity*, Vol. 5 (World scientific, Singapore, 1990).

[3] B. I. Halperin, Quantized Hall conductance, current-carrying edge states, and the existence of extended states in a two-dimensional disordered potential, Phys. Rev. B **25**, 2185 (1982).

[4] R. Laughlin, Superconducting ground state of noninteracting particles obeying fractional statistics, in *Ten Years of Superconductivity: 1980–1990* (Springer, New York, 1988), p. 313.

[5] A. C. Neto, F. Guinea, N. M. Peres, K. S. Novoselov, and A. K. Geim, The electronic properties of graphene, Rev. Mod. Phys. **81**, 109 (2009).
[6] P. R. Wallace, The band theory of graphite, Phys. Rev. **71**, 622 (1947).
[7] M. I. Katsnelson, K. S. Novoselov, and A. K. Geim, Chiral tunnelling and the Klein paradox in graphene, Nat. Phys. **2**, 620 (2006).
[8] A. F. Young and P. Kim, Quantum interference and Klein tunnelling in graphene heterojunctions, Nat. Phys. **5**, 222 (2009).
[9] A. K. Geim and K. S. Novoselov, The rise of graphene, in *Nanoscience and Technology: A Collection of Reviews from Nature Journals* (World Scientific, Singapore, 2010), p. 11.
[10] N. Stander, B. Huard, and D. Goldhaber-Gordon, Evidence for Klein Tunneling in Graphene p-n Junctions, Phys. Rev. Lett. **102**, 026807 (2009).
[11] M. Katsnelson, Zitterbewegung, chirality, and minimal conductivity in graphene, Eur. Phys. J. B **51**, 157 (2006).
[12] J. Tworzydło, B. Trauzettel, M. Titov, A. Rycerz, and C. W. Beenakker, Sub-Poissonian Shot Noise in Graphene, Phys. Rev. Lett. **96**, 246802 (2006).
[13] K. S. Novoselov, A. K. Geim, S. V. Morozov, D. Jiang, M. I. Katsnelson, I. Grigorieva, S. Dubonos, and A. Firsov, Two-dimensional gas of massless Dirac fermions in graphene, Nature (London) **438**, 197 (2005).
[14] R. R. Nair, P. Blake, A. N. Grigorenko, K. S. Novoselov, T. J. Booth, T. Stauber, N. M. Peres, and A. K. Geim, Fine structure constant defines visual transparency of graphene, Science **320**, 1308 (2008).
[15] D. Elias, R. Gorbachev, A. Mayorov, S. Morozov, A. Zhukov, P. Blake, L. Ponomarenko, I. Grigorieva, K. Novoselov, F. Guinea *et al.*, Dirac cones reshaped by interaction effects in suspended graphene, Nat. Phys. **7**, 701 (2011).
[16] M. A. Vozmediano and F. Guinea, Effect of Coulomb interactions on the physical observables of graphene, Phys. Scr. **2012**, 014015 (2012).
[17] C. D. Roberts and A. G. Williams, Dyson-Schwinger equations and their application to hadronic physics, Prog. Part. Nucl. Phys. **33**, 477 (1994).
[18] E. Marino, Quantum electrodynamics of particles on a plane and the Chern-Simons theory, Nucl. Phys. **B408**, 551 (1993).
[19] E. V. Gorbar, V. P. Gusynin, and V. A. Miransky, Dynamical chiral symmetry breaking on a brane in reduced QED, Phys. Rev. D **64**, 105028 (2001).
[20] M. Heydeman, C. B. Jepsen, Z. Ji, and A. Yarom, Renormalization and conformal invariance of non-local quantum electrodynamics, J. High Energy Phys. 08 (2020) 007.
[21] R. Do Amaral and E. Marino, Canonical quantization of theories containing fractional powers of the d'Alembertian operator, J. Phys. A **25**, 5183 (1992).
[22] E. Marino, L. O. Nascimento, V. S. Alves, and C. M. Smith, Unitarity of theories containing fractional powers of the d'Alembertian operator, Phys. Rev. D **90**, 105003 (2014).
[23] E. C. Marino, *Quantum Field Theory Approach to Condensed Matter Physics* (Cambridge University Press, Cambridge, England, 2017).
[24] E. Marino, L. O. Nascimento, V. S. Alves, and C. M. Smith, Interaction Induced Quantum Valley Hall Effect in Graphene, Phys. Rev. X **5**, 011040 (2015).
[25] J. D. L. Silva, A. N. Braga, W. P. Pires, V. S. Alves, D. T. Alves, and E. Marino, Inhibition of the Fermi velocity renormalization in a graphene sheet by the presence of a conducting plate, Nucl. Phys. **B920**, 221 (2017).
[26] W. P. Pires, J. D. L. Silva, A. N. Braga, V. S. Alves, D. T. Alves, and E. Marino, Cavity effects on the Fermi velocity renormalization in a graphene sheet, Nucl. Phys. **B932**, 529 (2018).
[27] G. D. Mahan, *Many-Particle Physics* (Springer Science & Business Media, New York, 2013).
[28] N. Menezes, V. S. Alves, E. Marino, L. Nascimento, L. O. Nascimento, and C. M. Smith, Spin g-factor due to electronic interactions in graphene, Phys. Rev. B **95**, 245138 (2017).
[29] V. S. Alves, W. S. Elias, L. O. Nascimento, V. Juričić, and F. Peña, Chiral symmetry breaking in the pseudoquantum electrodynamics, Phys. Rev. D **87**, 125002 (2013).
[30] L. O. Nascimento, V. S. Alves, F. Peña, C. M. Smith, and E. Marino, Chiral-symmetry breaking in pseudoquantum electrodynamics at finite temperature, Phys. Rev. D **92**, 025018 (2015).
[31] V. S. Alves, R. O. Junior, E. Marino, and L. O. Nascimento, Dynamical mass generation in pseudoquantum electrodynamics with four-fermion interactions, Phys. Rev. D **96**, 034005 (2017).
[32] L. O. Nascimento, Introduction to topological phases and electronic interactions in $(2+1)$ dimensions, Braz. J. Phys. **47**, 215 (2017).
[33] E. Marino, D. Niemeyer, V. S. Alves, T. H. Hansson, and S. Moroz, Screening and topological order in thin superconducting films, New J. Phys. **20**, 083049 (2018).
[34] E. Marino, L. O. Nascimento, V. S. Alves, N. Menezes, and C. M. Smith, Quantum-electrodynamical approach to the exciton spectrum in transition-metal dichalcogenides, 2D Mater. **5**, 041006 (2018).
[35] V. S. Alves, T. Macri, G. C. Magalhães, E. Marino, and L. O. Nascimento, Two-dimensional Yukawa interactions from nonlocal Proca quantum electrodynamics, Phys. Rev. D **97**, 096003 (2018).
[36] E. C. Marino, From graphene to quantum computation: An expedition to the Dirac sea, in *Strongly Coupled Field Theories for Condensed Matter and Quantum Information Theory* (Springer, New York, 2020), p. 339.
[37] G. C. Magalhães, V. S. Alves, E. C. Marino, and L. O. Nascimento, Pseudo quantum electrodynamics and Chern-Simons theory coupled to two-dimensional electrons, Phys. Rev. D **101**, 116005 (2020).
[38] E. Barnes, E. Hwang, R. Throckmorton, and S. D. Sarma, Effective field theory, three-loop perturbative expansion, and their experimental implications in graphene many-body effects, Phys. Rev. B **89**, 235431 (2014).
[39] J. González, F. Guinea, and M. Vozmediano, Non-fermi liquid behavior of electrons in the half-filled honeycomb lattice (a renormalization group approach), Nucl. Phys. **B424**, 595 (1994).

[40] F. de Juan, M. Sturla, and M. A. Vozmediano, Space Dependent Fermi Velocity in Strained Graphene, Phys. Rev. Lett. **108**, 227205 (2012).

[41] A. Raoux, M. Polini, R. Asgari, A. Hamilton, R. Fazio, and A. H. MacDonald, Velocity-modulation control of electron-wave propagation in graphene, Phys. Rev. B **81**, 073407 (2010).

[42] R. D. Pisarski, Chiral-symmetry breaking in three-dimensional electrodynamics, Phys. Rev. D **29**, 2423 (1984).

[43] T. W. Appelquist, Chiral symmetry breaking in quantum field theory, Prog. Theor. Phys. **85**, 244 (1985).

[44] I. Sodemann and M. M. Fogler, Interaction corrections to the polarization function of graphene, Phys. Rev. B **86**, 115408 (2012).

[45] E. A. Galapon, The Cauchy principal value and the Hadamard finite part integral as values of absolutely convergent integrals, J. Math. Phys. (N.Y.) **57**, 033502 (2016).

[46] V. N. Kotov, B. Uchoa, and A. C. Neto, Electron-electron interactions in the vacuum polarization of graphene, Phys. Rev. B **78**, 035119 (2008).

[47] E. Mishchenko, Minimal conductivity in graphene: Interaction corrections and ultraviolet anomaly, Europhys. Lett. **83**, 17005 (2008).

[48] T. Stauber, P. Parida, M. Trushin, M. V. Ulybyshev, D. L. Boyda, and J. Schliemann, Interacting Electrons in Graphene: Fermi Velocity Renormalization and Optical Response, Phys. Rev. Lett. **118**, 266801 (2017).

[49] R. Snieder and C. U. Press, *A Guided Tour of Mathematical Methods: For the Physical Sciences*, A Guided Tour of Mathematical Methods for the Physical Sciences (Cambridge University Press, Cambridge, England, 2004).

[50] P. A. D. Gonçalves and N. M. Peres, *An Introduction to Graphene Plasmonics* (World Scientific, Singapore, 2016).